

Eight-Node Solid Element for Thick Shell Simulations

Yong Guo

Livermore Software Technology Corporation
Livermore, California, USA

Abstract

An eight-node hexahedral solid element is incorporated into LS-DYNA to simulate thick shell structure. The element formulations are derived in a corotational coordinate system and the strain operator is calculated with a Taylor series expansion about the center of the element. Special treatments are made on the dilatational strain component and shear strain components to eliminate the volumetric and shear locking. The use of consistent tangential stiffness and geometric stiffness greatly improves the convergence rate in implicit analysis.

INTRODUCTION

Large scale finite element analyses are extensively used in engineering designs and process controls. For example, in automobile crashworthiness, hundreds of thousands of unknowns are involved in the computer simulation models, and in metal forming processing, tests in the design of new dies or new products are done by numerical computations instead of costly experiments. The efficiency of the elements is of crucial importance to speed up the design processes and reduce the computational costs for these problems. Over the past ten years considerable progress has been achieved in developing fast and reliable elements.

In the simulation of shell structures, Belytschko-Lin-Tsay (Belytschko, 1984a) and Hughes-Liu (Hughes, 1981a and 1981b) shell elements are widely used. However, in some cases thick shell elements are more suitable. For example, in the sheet metal forming with large curvature, traditional thin shell elements cannot give satisfactory results. Also thin shell elements cannot give us detailed strain information though the thickness. In LS-DYNA, the eight-node solid thick shell element is still based on the Hughes-Liu and Belytschko-Lin-Tsay shells (Hallquist, 1998). A new eight-node solid element based on Liu, 1985, 1994 and 1998 is incorporated into LS-DYNA, intended for thick shell simulation. The strain operator of this element is derived from a Taylor series expansion and special treatments on strain components are utilized to avoid volumetric and shear locking.

The organization of this paper is as follows. The element formulations are described in the next section. Several numerical problems are studied in the third section, followed by the conclusions.

ELEMENT FORMULATIONS

Strain Operator

The new element is based on the eight-node hexahedral element proposed and enhanced by Liu, 1985, 1994, 1998. For an eight-node hexahedral element, the spatial coordinates, x_i , and the velocity components, v_i , in the element are approximated in terms of nodal values, x_{ia} and v_{ia} ,

by

$$x_i = \sum_{a=1}^8 N_a(\xi, \eta, \zeta) x_{ia}, \quad (1)$$

$$v_i = \sum_{a=1}^8 N_a(\xi, \eta, \zeta) v_{ia}, \quad i = 1, 2, 3 \quad (2)$$

where the trilinear shape functions are expressed as

$$N_a(\xi, \eta, \zeta) = \frac{1}{8}(1 + \xi_a \xi)(1 + \eta_a \eta)(1 + \zeta_a \zeta) \quad (3)$$

and the subscripts i and a denote coordinate components ranging from one to three and the element nodal numbers ranging from one to eight, respectively. The referential coordinates ξ , η and ζ of node a are denoted by ξ_a , η_a and ζ_a , respectively.

The strain rate (or rate of deformation), $\dot{\epsilon}$, is composed of six components,

$$\dot{\epsilon}^t = [\epsilon_{xx} \quad \epsilon_{yy} \quad \epsilon_{zz} \quad \epsilon_{xy} \quad \epsilon_{yz} \quad \epsilon_{zx}] \quad (4)$$

and is related to the nodal velocities by a strain operator, $\bar{\mathbf{B}}$,

$$\dot{\epsilon} = \bar{\mathbf{B}}(\xi, \eta, \zeta) \mathbf{v}, \quad (5)$$

where

$$\mathbf{v}^t = [v_{x1} \quad v_{y1} \quad v_{z1} \quad \cdots \quad v_{x8} \quad v_{y8} \quad v_{z8}], \quad (6)$$

$$\bar{\mathbf{B}} = \begin{bmatrix} \bar{\mathbf{B}}_{xx} \\ \bar{\mathbf{B}}_{yy} \\ \bar{\mathbf{B}}_{zz} \\ \bar{\mathbf{B}}_{xy} \\ \bar{\mathbf{B}}_{yz} \\ \bar{\mathbf{B}}_{zx} \end{bmatrix} = \begin{bmatrix} B_1(1) & 0 & 0 & \cdots & B_1(8) & 0 & 0 \\ 0 & B_2(1) & 0 & \cdots & 0 & B_2(8) & 0 \\ 0 & 0 & B_3(1) & \cdots & 0 & 0 & B_3(8) \\ B_2(1) & B_1(1) & 0 & \cdots & B_2(8) & B_1(8) & 0 \\ 0 & B_3(1) & B_2(1) & \cdots & 0 & B_3(8) & B_2(8) \\ B_3(1) & 0 & B_1(1) & \cdots & B_3(8) & 0 & B_1(8) \end{bmatrix} \quad (7)$$

and \mathbf{B}_1 , \mathbf{B}_2 and \mathbf{B}_3 are gradient vectors,

$$\begin{bmatrix} \mathbf{B}_1 \\ \mathbf{B}_2 \\ \mathbf{B}_3 \end{bmatrix} = \begin{bmatrix} \mathbf{N}_{,x}(\xi, \eta, \zeta) \\ \mathbf{N}_{,y}(\xi, \eta, \zeta) \\ \mathbf{N}_{,z}(\xi, \eta, \zeta) \end{bmatrix}. \quad (8)$$

Unlike standard solid element where the strain operator is computed by differentiating the shape functions, the strain operator for this new element is expanded in a Taylor series about the element center up to bilinear terms as follows (Liu, 1994, 1998),

$$\begin{aligned} \bar{\mathbf{B}}(\xi, \eta, \zeta) &= \bar{\mathbf{B}}(\mathbf{0}) + \bar{\mathbf{B}}_{,\xi}(\mathbf{0}) \xi + \bar{\mathbf{B}}_{,\eta}(\mathbf{0}) \eta + \bar{\mathbf{B}}_{,\zeta}(\mathbf{0}) \zeta \\ &\quad + 2 [\bar{\mathbf{B}}_{,\xi\eta}(\mathbf{0}) \xi\eta + \bar{\mathbf{B}}_{,\eta\zeta}(\mathbf{0}) \eta\zeta + \bar{\mathbf{B}}_{,\zeta\xi}(\mathbf{0}) \zeta\xi]. \end{aligned} \quad (9)$$

The first term on the right-hand side of the above equation (9) corresponds to the constant strain rates evaluated at the central point and the remaining terms are linear and bilinear strain rate terms.

Let

$$\mathbf{x}_1^t = \mathbf{x}^t = [x_1 \ x_2 \ x_3 \ x_4 \ x_5 \ x_6 \ x_7 \ x_8], \quad (10)$$

$$\mathbf{x}_2^t = \mathbf{y}^t = [y_1 \ y_2 \ y_3 \ y_4 \ y_5 \ y_6 \ y_7 \ y_8], \quad (11)$$

$$\mathbf{x}_3^t = \mathbf{z}^t = [z_1 \ z_2 \ z_3 \ z_4 \ z_5 \ z_6 \ z_7 \ z_8], \quad (12)$$

$$\boldsymbol{\xi}^t = [-1 \ 1 \ 1 \ -1 \ -1 \ 1 \ 1 \ -1], \quad (13)$$

$$\boldsymbol{\eta}^t = [-1 \ -1 \ 1 \ 1 \ -1 \ -1 \ 1 \ 1], \quad (14)$$

$$\boldsymbol{\zeta}^t = [-1 \ -1 \ -1 \ -1 \ 1 \ 1 \ 1 \ 1], \quad (15)$$

the Jacobian matrix at the center of the element can be evaluated as

$$\mathbf{J}(\mathbf{0}) = [J_{ij}] = \frac{1}{8} \begin{bmatrix} \boldsymbol{\xi}^t \mathbf{x} & \boldsymbol{\xi}^t \mathbf{y} & \boldsymbol{\xi}^t \mathbf{z} \\ \boldsymbol{\eta}^t \mathbf{x} & \boldsymbol{\eta}^t \mathbf{y} & \boldsymbol{\eta}^t \mathbf{z} \\ \boldsymbol{\zeta}^t \mathbf{x} & \boldsymbol{\zeta}^t \mathbf{y} & \boldsymbol{\zeta}^t \mathbf{z} \end{bmatrix}; \quad (16)$$

the determinant of the Jacobian matrix is denoted by j_0 and the inverse matrix of $\mathbf{J}(\mathbf{0})$ is denoted by \mathbf{D}

$$\mathbf{D} = [D_{ij}] = \mathbf{J}^{-1}(\mathbf{0}). \quad (17)$$

The gradient vectors and their derivatives with respect to the natural coordinates at the center of the element are given as follows,

$$\mathbf{b}_1 = \mathbf{N}_{,x}(\mathbf{0}) = \frac{1}{8} [D_{11}\boldsymbol{\xi} + D_{12}\boldsymbol{\eta} + D_{13}\boldsymbol{\zeta}], \quad (18)$$

$$\mathbf{b}_2 = \mathbf{N}_{,y}(\mathbf{0}) = \frac{1}{8} [D_{21}\boldsymbol{\xi} + D_{22}\boldsymbol{\eta} + D_{23}\boldsymbol{\zeta}], \quad (19)$$

$$\mathbf{b}_3 = \mathbf{N}_{,z}(\mathbf{0}) = \frac{1}{8} [D_{31}\boldsymbol{\xi} + D_{32}\boldsymbol{\eta} + D_{33}\boldsymbol{\zeta}]. \quad (20)$$

$$\mathbf{b}_{1,\xi} = \mathbf{N}_{,x\xi}(\mathbf{0}) = \frac{1}{8} [D_{12}\gamma_1 + D_{13}\gamma_2], \quad (21)$$

$$\mathbf{b}_{2,\xi} = \mathbf{N}_{,y\xi}(\mathbf{0}) = \frac{1}{8} [D_{22}\gamma_1 + D_{23}\gamma_2], \quad (22)$$

$$\mathbf{b}_{3,\xi} = \mathbf{N}_{,z\xi}(\mathbf{0}) = \frac{1}{8} [D_{32}\gamma_1 + D_{33}\gamma_2], \quad (23)$$

$$\mathbf{b}_{1,\eta} = \mathbf{N}_{,x\eta}(\mathbf{0}) = \frac{1}{8} [D_{11}\gamma_1 + D_{13}\gamma_3], \quad (24)$$

$$\mathbf{b}_{2,\eta} = \mathbf{N}_{,y\eta}(\mathbf{0}) = \frac{1}{8} [D_{21}\gamma_1 + D_{23}\gamma_3], \quad (25)$$

$$\mathbf{b}_{3,\eta} = \mathbf{N}_{,z\eta}(\mathbf{0}) = \frac{1}{8} [D_{31}\gamma_1 + D_{33}\gamma_3], \quad (26)$$

$$\mathbf{b}_{1,\zeta} = \mathbf{N}_{,x\zeta}(\mathbf{0}) = \frac{1}{8} [D_{11}\gamma_2 + D_{12}\gamma_3], \quad (27)$$

$$\mathbf{b}_{2,\zeta} = \mathbf{N}_{,y\zeta}(\mathbf{0}) = \frac{1}{8} [D_{21}\gamma_2 + D_{22}\gamma_3], \quad (28)$$

$$\mathbf{b}_{3,\zeta} = \mathbf{N}_{,z\zeta}(\mathbf{0}) = \frac{1}{8} [D_{31}\gamma_2 + D_{32}\gamma_3], \quad (29)$$

$$\mathbf{b}_{1,\xi\eta} = \mathbf{N}_{,x\xi\eta}(\mathbf{0}) = \frac{1}{8} [D_{13}\gamma_4 - (\mathbf{p}_1^t \mathbf{x}_i) \mathbf{b}_{i,\xi} - (\mathbf{r}_1^t \mathbf{x}_i) \mathbf{b}_{i,\eta}], \quad (30)$$

$$\mathbf{b}_{2,\xi\eta} = \mathbf{N}_{,y\xi\eta}(\mathbf{0}) = \frac{1}{8} [D_{23}\gamma_4 - (\mathbf{p}_2^t \mathbf{x}_i) \mathbf{b}_{i,\xi} - (\mathbf{r}_2^t \mathbf{x}_i) \mathbf{b}_{i,\eta}], \quad (31)$$

$$\mathbf{b}_{3,\xi\eta} = \mathbf{N}_{,z\xi\eta}(\mathbf{0}) = \frac{1}{8} [D_{33}\gamma_4 - (\mathbf{p}_3^t \mathbf{x}_i) \mathbf{b}_{i,\xi} - (\mathbf{r}_3^t \mathbf{x}_i) \mathbf{b}_{i,\eta}], \quad (32)$$

$$\mathbf{b}_{1,\eta\zeta} = \mathbf{N}_{,x\eta\zeta}(\mathbf{0}) = \frac{1}{8} [D_{11}\gamma_4 - (\mathbf{q}_1^t \mathbf{x}_i) \mathbf{b}_{i,\eta} - (\mathbf{p}_1^t \mathbf{x}_i) \mathbf{b}_{i,\zeta}], \quad (33)$$

$$\mathbf{b}_{2,\eta\zeta} = \mathbf{N}_{,y\eta\zeta}(\mathbf{0}) = \frac{1}{8} [D_{21}\gamma_4 - (\mathbf{q}_2^t \mathbf{x}_i) \mathbf{b}_{i,\eta} - (\mathbf{p}_2^t \mathbf{x}_i) \mathbf{b}_{i,\zeta}], \quad (34)$$

$$\mathbf{b}_{3,\eta\zeta} = \mathbf{N}_{,z\eta\zeta}(\mathbf{0}) = \frac{1}{8} [D_{31}\gamma_4 - (\mathbf{q}_3^t \mathbf{x}_i) \mathbf{b}_{i,\eta} - (\mathbf{p}_3^t \mathbf{x}_i) \mathbf{b}_{i,\zeta}], \quad (35)$$

$$\mathbf{b}_{1,\zeta\xi} = \mathbf{N}_{,x\zeta\xi}(\mathbf{0}) = \frac{1}{8} [D_{12}\gamma_4 - (\mathbf{r}_1^t \mathbf{x}_i) \mathbf{b}_{i,\zeta} - (\mathbf{q}_1^t \mathbf{x}_i) \mathbf{b}_{i,\xi}], \quad (36)$$

$$\mathbf{b}_{2,\zeta\xi} = \mathbf{N}_{,y\zeta\xi}(\mathbf{0}) = \frac{1}{8} [D_{22}\gamma_4 - (\mathbf{r}_2^t \mathbf{x}_i) \mathbf{b}_{i,\zeta} - (\mathbf{q}_2^t \mathbf{x}_i) \mathbf{b}_{i,\xi}], \quad (37)$$

$$\mathbf{b}_{3,\zeta\xi} = \mathbf{N}_{,z\zeta\xi}(\mathbf{0}) = \frac{1}{8} [D_{32}\gamma_4 - (\mathbf{r}_3^t \mathbf{x}_i) \mathbf{b}_{i,\zeta} - (\mathbf{q}_3^t \mathbf{x}_i) \mathbf{b}_{i,\xi}], \quad (38)$$

where

$$\mathbf{p}_i = D_{i1}\mathbf{h}_1 + D_{i3}\mathbf{h}_3, \quad (39)$$

$$\mathbf{q}_i = D_{i1}\mathbf{h}_2 + D_{i2}\mathbf{h}_3, \quad (40)$$

$$\mathbf{r}_i = D_{i2}\mathbf{h}_1 + D_{i3}\mathbf{h}_2, \quad (41)$$

$$\gamma_\alpha = \mathbf{h}_\alpha - (\mathbf{h}_\alpha^t \mathbf{x}_i) \mathbf{b}_i, \quad (42)$$

and

$$\mathbf{h}_1^t = [1 \ -1 \ 1 \ -1 \ 1 \ -1 \ 1 \ -1], \quad (43)$$

$$\mathbf{h}_2^t = [1 \ -1 \ -1 \ 1 \ -1 \ 1 \ 1 \ -1], \quad (44)$$

$$\mathbf{h}_3^t = [1 \ 1 \ -1 \ -1 \ -1 \ -1 \ 1 \ 1], \quad (45)$$

$$\mathbf{h}_4^t = [-1 \ 1 \ -1 \ 1 \ 1 \ -1 \ 1 \ -1]. \quad (46)$$

In the above equations \mathbf{h}_1 is the $\xi\eta$ -hourglass vector, \mathbf{h}_2 the $\eta\zeta$ -hourglass vector, \mathbf{h}_3 the $\zeta\xi$ -hourglass vector and \mathbf{h}_4 the $\xi\eta\zeta$ -hourglass vector. They are the zero energy-deformation modes associated with the one-point-quadrature element which result in a non-constant strain field in the element (Flanagan, 1981, Belytschko, 1984 and Liu, 1984). The γ_α in equations (21)–(38) are the stabilization vectors. They are orthogonal to the linear displacement field and provide a consistent stabilization for the element.

The strain operators, $\overline{\mathbf{B}}(\xi, \eta, \zeta)$, can be decomposed into two parts, the dilatational part, $\overline{\mathbf{B}}^{\text{dil}}(\xi, \eta, \zeta)$, and the deviatoric part, $\overline{\mathbf{B}}^{\text{dev}}(\xi, \eta, \zeta)$, both of which can be expanded about the element center as in equation (9)

$$\begin{aligned} \overline{\mathbf{B}}^{\text{dil}}(\xi, \eta, \zeta) &= \overline{\mathbf{B}}^{\text{dil}}(\mathbf{0}) + \overline{\mathbf{B}}_{,\xi}^{\text{dil}}(\mathbf{0}) \xi + \overline{\mathbf{B}}_{,\eta}^{\text{dil}}(\mathbf{0}) \eta + \overline{\mathbf{B}}_{,\zeta}^{\text{dil}}(\mathbf{0}) \zeta \\ &\quad + 2[\overline{\mathbf{B}}_{,\xi\eta}^{\text{dil}}(\mathbf{0}) \xi\eta + \overline{\mathbf{B}}_{,\eta\zeta}^{\text{dil}}(\mathbf{0}) \eta\zeta + \overline{\mathbf{B}}_{,\zeta\xi}^{\text{dil}}(\mathbf{0}) \zeta\xi], \end{aligned} \quad (47)$$

$$\begin{aligned} \overline{\mathbf{B}}^{\text{dev}}(\xi, \eta, \zeta) &= \overline{\mathbf{B}}^{\text{dev}}(\mathbf{0}) + \overline{\mathbf{B}}_{,\xi}^{\text{dev}}(\mathbf{0}) \xi + \overline{\mathbf{B}}_{,\eta}^{\text{dev}}(\mathbf{0}) \eta + \overline{\mathbf{B}}_{,\zeta}^{\text{dev}}(\mathbf{0}) \zeta \\ &\quad + 2[\overline{\mathbf{B}}_{,\xi\eta}^{\text{dev}}(\mathbf{0}) \xi\eta + \overline{\mathbf{B}}_{,\eta\zeta}^{\text{dev}}(\mathbf{0}) \eta\zeta + \overline{\mathbf{B}}_{,\zeta\xi}^{\text{dev}}(\mathbf{0}) \zeta\xi]. \end{aligned} \quad (48)$$

To avoid volumetric locking, the dilatational part of the strain operators is evaluated only at one quadrature point, the center of the element, i.e., they are constant terms

$$\overline{\mathbf{B}}^{\text{dil}}(\xi, \eta, \zeta) = \overline{\mathbf{B}}^{\text{dil}}(\mathbf{0}). \quad (49)$$

To remove shear locking, the deviatoric strain submatrices can be written in an orthogonal corotational coordinate system rotating with the element as

$$\begin{aligned} \overline{\mathbf{B}}_{xx}^{\text{dev}}(\xi, \eta, \zeta) &= \overline{\mathbf{B}}_{xx}^{\text{dev}}(\mathbf{0}) + \overline{\mathbf{B}}_{xx,\xi}^{\text{dev}}(\mathbf{0})\xi + \overline{\mathbf{B}}_{xx,\eta}^{\text{dev}}(\mathbf{0})\eta + \overline{\mathbf{B}}_{xx,\zeta}^{\text{dev}}(\mathbf{0})\zeta \\ &\quad + 2[\overline{\mathbf{B}}_{xx,\xi\eta}^{\text{dev}}(\mathbf{0})\xi\eta + \overline{\mathbf{B}}_{xx,\eta\zeta}^{\text{dev}}(\mathbf{0})\eta\zeta + \overline{\mathbf{B}}_{xx,\zeta\xi}^{\text{dev}}(\mathbf{0})\zeta\xi], \end{aligned} \quad (50)$$

$$\begin{aligned} \overline{\mathbf{B}}_{yy}^{\text{dev}}(\xi, \eta, \zeta) &= \overline{\mathbf{B}}_{yy}^{\text{dev}}(\mathbf{0}) + \overline{\mathbf{B}}_{yy,\xi}^{\text{dev}}(\mathbf{0})\xi + \overline{\mathbf{B}}_{yy,\eta}^{\text{dev}}(\mathbf{0})\eta + \overline{\mathbf{B}}_{yy,\zeta}^{\text{dev}}(\mathbf{0})\zeta \\ &\quad + 2[\overline{\mathbf{B}}_{yy,\xi\eta}^{\text{dev}}(\mathbf{0})\xi\eta + \overline{\mathbf{B}}_{yy,\eta\zeta}^{\text{dev}}(\mathbf{0})\eta\zeta + \overline{\mathbf{B}}_{yy,\zeta\xi}^{\text{dev}}(\mathbf{0})\zeta\xi], \end{aligned} \quad (51)$$

$$\begin{aligned} \overline{\mathbf{B}}_{zz}^{\text{dev}}(\xi, \eta, \zeta) &= \overline{\mathbf{B}}_{zz}^{\text{dev}}(\mathbf{0}) + \overline{\mathbf{B}}_{zz,\xi}^{\text{dev}}(\mathbf{0})\xi + \overline{\mathbf{B}}_{zz,\eta}^{\text{dev}}(\mathbf{0})\eta + \overline{\mathbf{B}}_{zz,\zeta}^{\text{dev}}(\mathbf{0})\zeta \\ &\quad + 2[\overline{\mathbf{B}}_{zz,\xi\eta}^{\text{dev}}(\mathbf{0})\xi\eta + \overline{\mathbf{B}}_{zz,\eta\zeta}^{\text{dev}}(\mathbf{0})\eta\zeta + \overline{\mathbf{B}}_{zz,\zeta\xi}^{\text{dev}}(\mathbf{0})\zeta\xi], \end{aligned} \quad (52)$$

$$\overline{\mathbf{B}}_{xy}^{\text{dev}}(\xi, \eta, \zeta) = \overline{\mathbf{B}}_{xy}^{\text{dev}}(\mathbf{0}) + \overline{\mathbf{B}}_{xy,\zeta}^{\text{dev}}(\mathbf{0})\zeta, \quad (53)$$

$$\overline{\mathbf{B}}_{yz}^{\text{dev}}(\xi, \eta, \zeta) = \overline{\mathbf{B}}_{yz}^{\text{dev}}(\mathbf{0}) + \overline{\mathbf{B}}_{yz,\xi}^{\text{dev}}(\mathbf{0})\xi, \quad (54)$$

$$\overline{\mathbf{B}}_{zx}^{\text{dev}}(\xi, \eta, \zeta) = \overline{\mathbf{B}}_{zx}^{\text{dev}}(\mathbf{0}) + \overline{\mathbf{B}}_{zx,\eta}^{\text{dev}}(\mathbf{0})\eta. \quad (55)$$

Here, only one linear term is left for shear strain components such that the modes causing shear locking are removed. The normal strain components keep all non-constant terms given in equation (48).

Summation of equation (49) and equations (50)–(55) yields the following strain submatrices which can eliminate the shear and volumetric locking:

$$\begin{aligned} \overline{\mathbf{B}}_{xx}(\xi, \eta, \zeta) &= \overline{\mathbf{B}}_{xx}(\mathbf{0}) + \overline{\mathbf{B}}_{xx,\xi}^{\text{dev}}(\mathbf{0})\xi + \overline{\mathbf{B}}_{xx,\eta}^{\text{dev}}(\mathbf{0})\eta + \overline{\mathbf{B}}_{xx,\zeta}^{\text{dev}}(\mathbf{0})\zeta \\ &\quad + 2[\overline{\mathbf{B}}_{xx,\xi\eta}^{\text{dev}}(\mathbf{0})\xi\eta + \overline{\mathbf{B}}_{xx,\eta\zeta}^{\text{dev}}(\mathbf{0})\eta\zeta + \overline{\mathbf{B}}_{xx,\zeta\xi}^{\text{dev}}(\mathbf{0})\zeta\xi], \end{aligned} \quad (56)$$

$$\begin{aligned} \overline{\mathbf{B}}_{yy}(\xi, \eta, \zeta) &= \overline{\mathbf{B}}_{yy}(\mathbf{0}) + \overline{\mathbf{B}}_{yy,\xi}^{\text{dev}}(\mathbf{0})\xi + \overline{\mathbf{B}}_{yy,\eta}^{\text{dev}}(\mathbf{0})\eta + \overline{\mathbf{B}}_{yy,\zeta}^{\text{dev}}(\mathbf{0})\zeta \\ &\quad + 2[\overline{\mathbf{B}}_{yy,\xi\eta}^{\text{dev}}(\mathbf{0})\xi\eta + \overline{\mathbf{B}}_{yy,\eta\zeta}^{\text{dev}}(\mathbf{0})\eta\zeta + \overline{\mathbf{B}}_{yy,\zeta\xi}^{\text{dev}}(\mathbf{0})\zeta\xi], \end{aligned} \quad (57)$$

$$\begin{aligned} \overline{\mathbf{B}}_{zz}(\xi, \eta, \zeta) &= \overline{\mathbf{B}}_{zz}(\mathbf{0}) + \overline{\mathbf{B}}_{zz,\xi}^{\text{dev}}(\mathbf{0})\xi + \overline{\mathbf{B}}_{zz,\eta}^{\text{dev}}(\mathbf{0})\eta + \overline{\mathbf{B}}_{zz,\zeta}^{\text{dev}}(\mathbf{0})\zeta \\ &\quad + 2[\overline{\mathbf{B}}_{zz,\xi\eta}^{\text{dev}}(\mathbf{0})\xi\eta + \overline{\mathbf{B}}_{zz,\eta\zeta}^{\text{dev}}(\mathbf{0})\eta\zeta + \overline{\mathbf{B}}_{zz,\zeta\xi}^{\text{dev}}(\mathbf{0})\zeta\xi], \end{aligned} \quad (58)$$

$$\overline{\mathbf{B}}_{xy}(\xi, \eta, \zeta) = \overline{\mathbf{B}}_{xy}(\mathbf{0}) + \overline{\mathbf{B}}_{xy,\zeta}^{\text{dev}}(\mathbf{0})\zeta, \quad (59)$$

$$\overline{\mathbf{B}}_{yz}(\xi, \eta, \zeta) = \overline{\mathbf{B}}_{yz}(\mathbf{0}) + \overline{\mathbf{B}}_{yz,\xi}^{\text{dev}}(\mathbf{0})\xi, \quad (60)$$

$$\overline{\mathbf{B}}_{zx}(\xi, \eta, \zeta) = \overline{\mathbf{B}}_{zx}(\mathbf{0}) + \overline{\mathbf{B}}_{zx,\eta}^{\text{dev}}(\mathbf{0})\eta. \quad (61)$$

It is noted that the elements developed above can not pass the patch test if the elements are skewed. To remedy this drawback, the gradient vectors defined in (18)–(20) are replaced by the uniform gradient matrices, proposed by Flanagan, 1981,

$$\begin{bmatrix} \tilde{\mathbf{b}}_1 \\ \tilde{\mathbf{b}}_2 \\ \tilde{\mathbf{b}}_3 \end{bmatrix} = \frac{1}{V_e} \int_{\Omega_e} \begin{bmatrix} \mathbf{B}_1(\xi, \eta, \zeta) \\ \mathbf{B}_2(\xi, \eta, \zeta) \\ \mathbf{B}_3(\xi, \eta, \zeta) \end{bmatrix} dV, \quad (62)$$

where V_e is the element volume and the stabilization vectors are redefined as

$$\tilde{\gamma}_\alpha = \mathbf{h}_\alpha - (\mathbf{h}_\alpha^t \mathbf{x}_i) \tilde{\mathbf{b}}_i. \quad (63)$$

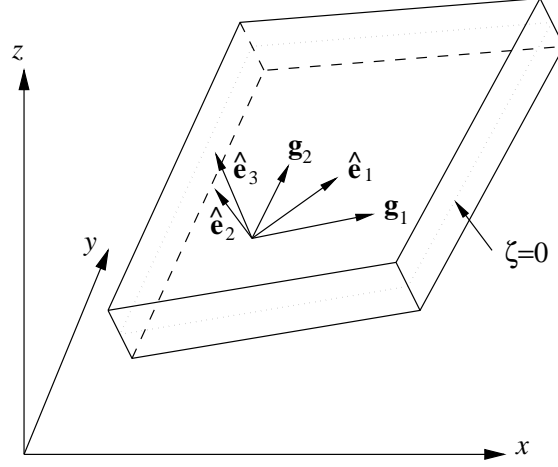


Figure 1: Definition of corotational coordinate system

The element using the strain submatrices (56)-(61) and uniform gradient matrices (62) with four point quadrature scheme is called HEXDS element.

Corotational Coordinate System

In elements for shell/plate structure simulations, the elimination of the shear locking depends on the proper treatment of the shear strain. It is necessary to attach a local coordinate system to the element so that the strain tensor in this local system is relevant for the treatment. The corotational coordinate system determined here is one of the most convenient ways to define such a local system.

A corotational coordinate system is defined as a Cartesian coordinate system which rotates with the element. Let $\{x_a, y_a, z_a\}$ denote the current nodal spatial coordinates in the global system. For each quadrature point with natural coordinates (ξ, η, ζ) , we can have two tangent directions on the midsurface ($\zeta = 0$) within the element (see Fig. 1)

$$\mathbf{g}_1 = \frac{\partial \mathbf{x}}{\partial \xi} = \begin{bmatrix} \frac{\partial x}{\partial \xi} & \frac{\partial y}{\partial \xi} & \frac{\partial z}{\partial \xi} \end{bmatrix} = [N_{a,\xi} x_a \quad N_{a,\xi} y_a \quad N_{a,\xi} z_a]_{(\xi,\eta,0)}, \quad (64)$$

$$\mathbf{g}_2 = \frac{\partial \mathbf{x}}{\partial \eta} = \begin{bmatrix} \frac{\partial x}{\partial \eta} & \frac{\partial y}{\partial \eta} & \frac{\partial z}{\partial \eta} \end{bmatrix} = [N_{a,\eta} x_a \quad N_{a,\eta} y_a \quad N_{a,\eta} z_a]_{(\xi,\eta,0)}. \quad (65)$$

The unit vector $\hat{\mathbf{e}}_1$ of the corotational coordinate system is defined as the bisector of the angle intersected by these two tangent vectors \mathbf{g}_1 and \mathbf{g}_2 ; the unit vector $\hat{\mathbf{e}}_3$ is perpendicular to the midsurface and the other unit vector is determined by $\hat{\mathbf{e}}_1$ and $\hat{\mathbf{e}}_3$, i.e.,

$$\hat{\mathbf{e}}_1 = \left(\frac{\mathbf{g}_1}{|\mathbf{g}_1|} + \frac{\mathbf{g}_2}{|\mathbf{g}_2|} \right) / \left| \frac{\mathbf{g}_1}{|\mathbf{g}_1|} + \frac{\mathbf{g}_2}{|\mathbf{g}_2|} \right|, \quad (66)$$

$$\hat{\mathbf{e}}_3 = \frac{\mathbf{g}_1 \times \mathbf{g}_2}{|\mathbf{g}_1 \times \mathbf{g}_2|}, \quad (67)$$

$$\hat{\mathbf{e}}_2 = \hat{\mathbf{e}}_3 \times \hat{\mathbf{e}}_1, \quad (68)$$

which lead to the transformation matrix

$$\mathbf{R} = \begin{bmatrix} \hat{\mathbf{e}}_1 \\ \hat{\mathbf{e}}_2 \\ \hat{\mathbf{e}}_3 \end{bmatrix}. \quad (69)$$

Stress and Strain Measures

Since the corotational coordinate system rotates with the configuration, the stress defined in this corotational system does not change with the rotation or translation of the material body and is thus objective. Therefore, we use the Cauchy stress in the corotational coordinate system, called the corotational Cauchy stress, as our stress measure.

The rate of deformation (or velocity strain tensor), also defined in the corotational coordinate system, is used as the measure of the strain rate,

$$\dot{\hat{\epsilon}} = \hat{\mathbf{d}} = \frac{1}{2} \left[\frac{\partial \hat{\mathbf{v}}^{\text{def}}}{\partial \hat{\mathbf{x}}} + \left(\frac{\partial \hat{\mathbf{v}}^{\text{def}}}{\partial \hat{\mathbf{x}}} \right)^t \right], \quad (70)$$

where $\hat{\mathbf{v}}^{\text{def}}$ is the deformation part of the velocity in the corotational system $\hat{\mathbf{x}}$. If the initial strain $\hat{\epsilon}(\mathbf{X}, 0)$ is given, the strain tensor can be expressed as,

$$\hat{\epsilon}(\mathbf{X}, t) = \hat{\epsilon}(\mathbf{X}, 0) + \int_0^t \hat{\mathbf{d}}(\mathbf{X}, \tau) d\tau. \quad (71)$$

The strain increment is then given by the mid-point integration of the velocity strain tensor,

$$\Delta \hat{\epsilon} = \int_{t_n}^{t_{n+1}} \hat{\mathbf{d}} d\tau \doteq \frac{1}{2} \left[\frac{\partial \Delta \hat{\mathbf{u}}^{\text{def}}}{\partial \hat{\mathbf{x}}_{n+\frac{1}{2}}} + \left(\frac{\partial \Delta \hat{\mathbf{u}}^{\text{def}}}{\partial \hat{\mathbf{x}}_{n+\frac{1}{2}}} \right)^t \right], \quad (72)$$

where $\Delta \hat{\mathbf{u}}^{\text{def}}$ is the deformation part of the displacement increment in the corotational system $\hat{\mathbf{x}}_{n+\frac{1}{2}}$ referred to the mid-point configuration.

Corotational Stress and Strain Updates

For stress and strain updates, we assume that all variables at the previous time step t_n are known. Since the stress and strain measures defined in the earlier section are objective in the corotational system, we only need to calculate the strain increment from the displacement field within the time increment $[t_n, t_{n+1}]$. The stress is then updated by using the radial return algorithm.

All the kinematical quantities must be computed from the last time step configuration, Ω_n , at $t = t_n$ and the current configuration, Ω_{n+1} , at $t = t_{n+1}$ since these are the only available data. Denoting the spatial coordinates of these two configurations as \mathbf{x}_n and \mathbf{x}_{n+1} in the fixed global Cartesian coordinate system $O\mathbf{x}$, as shown in Fig. 2, the coordinates in the corresponding corotational Cartesian coordinate systems, $O\hat{\mathbf{x}}_n$ and $O\hat{\mathbf{x}}_{n+1}$, can be obtained by the following transformation rules:

$$\hat{\mathbf{x}}_n = \mathbf{R}_n \mathbf{x}_n, \quad (73)$$

$$\hat{\mathbf{x}}_{n+1} = \mathbf{R}_{n+1} \mathbf{x}_{n+1}, \quad (74)$$

where \mathbf{R}_n and \mathbf{R}_{n+1} are the orthogonal transformation matrices which rotate the global coordinate system to the corresponding corotational coordinate systems, respectively.

Since the strain increment is referred to the configuration at $t = t_{n+\frac{1}{2}}$, by assuming the velocities within the time increment $[t_n, t_{n+1}]$ are constant, we have

$$\mathbf{x}_{n+\frac{1}{2}} = \frac{1}{2} (\mathbf{x}_n + \mathbf{x}_{n+1}), \quad (75)$$

and the transformation to the corotational system associated with this mid-point configuration, $\Omega_{n+\frac{1}{2}}$, is given by

$$\hat{\mathbf{x}}_{n+\frac{1}{2}} = \mathbf{R}_{n+\frac{1}{2}} \mathbf{x}_{n+\frac{1}{2}}. \quad (76)$$

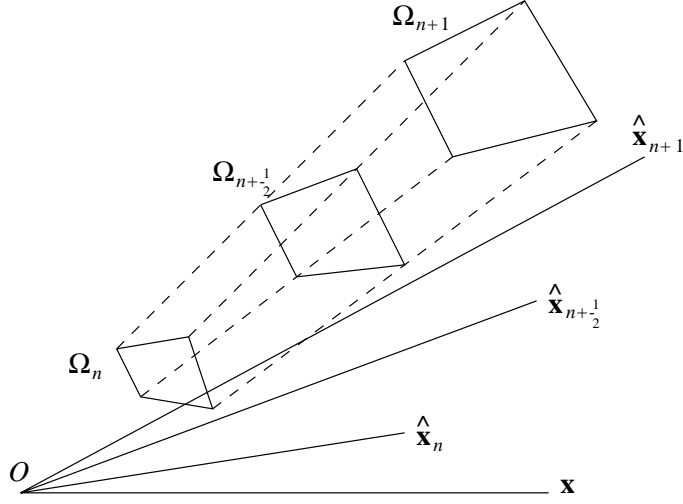


Figure 2: Configurations at times t_n , $t_{n+\frac{1}{2}}$ and t_{n+1}

Similar to polar decomposition, an incremental deformation can be separated into the summation of a pure deformation and a pure rotation (Belytschko, 1973). Letting $\Delta \mathbf{u}$ indicate the displacement increment within the time increment $[t_n, t_{n+1}]$, we write

$$\Delta \mathbf{u} = \Delta \mathbf{u}^{\text{def}} + \Delta \mathbf{u}^{\text{rot}}, \quad (77)$$

where $\Delta \mathbf{u}^{\text{def}}$ and $\Delta \mathbf{u}^{\text{rot}}$ are, respectively, the deformation part and the pure rotation part of the displacement increment in the global coordinate system. The deformation part also includes the translation displacements which cause no strains.

In order to obtain the deformation part of the displacement increment referred to the configuration at $t = t_{n+\frac{1}{2}}$, we need to find the rigid rotation from Ω_n to Ω_{n+1} provided that the mid-point configuration, $\Omega_{n+\frac{1}{2}}$, is held still. Defining two virtual configurations, Ω'_n and Ω'_{n+1} , by rotating the element bodies Ω_n and Ω_{n+1} into the corotational system $O\hat{\mathbf{x}}_{n+\frac{1}{2}}$ (Fig. 3) and denoting $\hat{\mathbf{x}}'_n$ and $\hat{\mathbf{x}}'_{n+1}$ as the coordinates of Ω'_n and Ω'_{n+1} in the corotational system $O\hat{\mathbf{x}}_{n+\frac{1}{2}}$, we have

$$\hat{\mathbf{x}}'_n = \hat{\mathbf{x}}_n, \quad \hat{\mathbf{x}}'_{n+1} = \hat{\mathbf{x}}_{n+1}. \quad (78)$$

We can see that from Ω_n to Ω'_n and from Ω'_{n+1} to Ω_{n+1} , the body experiences two rigid rotations and the rotation displacements are given by

$$\Delta \mathbf{u}_1^{\text{rot}} = \mathbf{x}'_n - \mathbf{x}_n = \mathbf{R}_{n+\frac{1}{2}}^t \hat{\mathbf{x}}'_n - \mathbf{x}_n = \mathbf{R}_{n+\frac{1}{2}}^t \hat{\mathbf{x}}_n - \mathbf{x}_n, \quad (79)$$

$$\Delta \mathbf{u}_2^{\text{rot}} = \mathbf{x}_{n+1} - \mathbf{x}'_{n+1} = \mathbf{x}_{n+1} - \mathbf{R}_{n+\frac{1}{2}}^t \hat{\mathbf{x}}'_{n+1} = \mathbf{x}_{n+1} - \mathbf{R}_{n+\frac{1}{2}}^t \hat{\mathbf{x}}_{n+1}. \quad (80)$$

Thus the total rotation displacement increment can be expressed as

$$\begin{aligned} \Delta \mathbf{u}^{\text{rot}} &= \Delta \mathbf{u}_1^{\text{rot}} + \Delta \mathbf{u}_2^{\text{rot}} = \mathbf{x}_{n+1} - \mathbf{x}_n - \mathbf{R}_{n+\frac{1}{2}}^t (\hat{\mathbf{x}}_{n+1} - \hat{\mathbf{x}}_n) \\ &= \Delta \mathbf{u} - \mathbf{R}_{n+\frac{1}{2}}^t (\hat{\mathbf{x}}_{n+1} - \hat{\mathbf{x}}_n). \end{aligned} \quad (81)$$

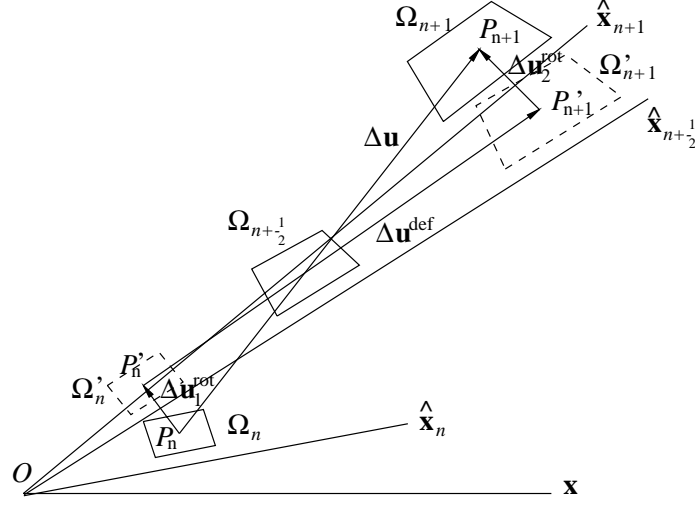


Figure 3: Separation of the displacement increment

Then the deformation part of the displacement increment referred to the configuration $\Omega_{n+\frac{1}{2}}$ is

$$\Delta \mathbf{u}^{\text{def}} = \Delta \mathbf{u} - \Delta \mathbf{u}^{\text{rot}} = \mathbf{R}_{n+\frac{1}{2}}^t (\hat{\mathbf{x}}_{n+1} - \hat{\mathbf{x}}_n). \quad (82)$$

Therefore, the deformation displacement increment in the corotational coordinate system $O\hat{\mathbf{x}}_{n+\frac{1}{2}}$ is obtained as

$$\Delta \hat{\mathbf{u}}^{\text{def}} = \mathbf{R}_{n+\frac{1}{2}} \Delta \mathbf{u}^{\text{def}} = \hat{\mathbf{x}}_{n+1} - \hat{\mathbf{x}}_n. \quad (83)$$

Once the strain increment is obtained by (72), the stress increment, also referred to the mid-point configuration $\Omega_{n+\frac{1}{2}}$, can be calculated with the radial return algorithm. The total strain and stress can then be updated as

$$\hat{\boldsymbol{\varepsilon}}_{n+1} = \hat{\boldsymbol{\varepsilon}}_n + \Delta \hat{\boldsymbol{\varepsilon}}, \quad (84)$$

$$\hat{\boldsymbol{\sigma}}_{n+1} = \hat{\boldsymbol{\sigma}}_n + \Delta \hat{\boldsymbol{\sigma}}. \quad (85)$$

Note that the resultant stress and strain tensors are both referred to the current configuration and defined in the current corotational coordinate system. By using the tensor transformation rule we can have the strain and stress components in the global coordinate system.

Tangent Stiffness Matrix and Nodal Force Vectors

From the Hu-Washizu variational principle, at both ν th and $(\nu + 1)$ th iteration, we have

$$\int_{\hat{\Omega}^\nu} \delta \hat{\varepsilon}_{ij}^\nu \hat{\sigma}_{ij}^\nu dV = \delta \hat{\pi}_{\text{ext}}^\nu, \quad (86)$$

$$\int_{\hat{\Omega}^{\nu+1}} \delta \hat{\varepsilon}_{ij}^{\nu+1} \hat{\sigma}_{ij}^{\nu+1} dV = \delta \hat{\pi}_{\text{ext}}^{\nu+1}, \quad (87)$$

where $\delta \hat{\pi}_{\text{ext}}$ is the virtual work done by the external forces. Note that both equations are written in the corotational coordinate system defined in the ν th iterative configuration given by \mathbf{x}_{n+1}^ν . The variables in this section are within the time step $[t_n, t_{n+1}]$ and superscripts indicate the number of iterations.

Assuming that all external forces are deformation-independent, linearization of (87) gives (Liu, 1992)

$$\int_{\hat{\Omega}^\nu} \delta \hat{u}_{i,j}^\nu \hat{C}_{ijkl}^\nu \Delta \hat{u}_{k,l} dV + \int_{\hat{\Omega}^\nu} \delta \hat{u}_{i,j}^\nu \hat{T}_{ijkl}^\nu \Delta \hat{u}_{k,l} dV = \delta \hat{\pi}_{\text{ext}}^{\nu+1} - \delta \hat{\pi}_{\text{ext}}^\nu, \quad (88)$$

where the Green-Naghdi rate of Cauchy stress tensor is used, i.e.,

$$\hat{T}_{ijkl}^\nu = \delta_{ik} \hat{\sigma}_{jl}^\nu. \quad (89)$$

The first term on the left hand side of (88) denotes the material response since it is due to pure deformation or stretching; the second term is an initial stress part resulting from finite deformation effect.

Taking account of the residual of the previous iteration, equation (87) can be approximated as

$$\int_{\hat{\Omega}^\nu} \delta \hat{u}_{i,j}^\nu \left(\hat{C}_{ijkl}^\nu + \hat{T}_{ijkl}^\nu \right) \Delta \hat{u}_{k,l} dV = \delta \hat{\pi}_{\text{ext}}^{\nu+1} - \int_{\hat{\Omega}^\nu} \delta \hat{\varepsilon}_{ij}^\nu \hat{\sigma}_{ij}^\nu dV. \quad (90)$$

If the strain and stress vectors are defined as

$$\boldsymbol{\varepsilon}^t = [\varepsilon_x \ \varepsilon_y \ \varepsilon_z \ 2\varepsilon_{xy} \ 2\varepsilon_{yz} \ 2\varepsilon_{zx} \ 2\omega_{xy} \ 2\omega_{yz} \ 2\omega_{zx}], \quad (91)$$

$$\boldsymbol{\sigma}^t = [\sigma_x \ \sigma_y \ \sigma_z \ \sigma_{xy} \ \sigma_{yz} \ \sigma_{zx}], \quad (92)$$

we can rewrite (90) as

$$\int_{\hat{\Omega}^\nu} \delta \hat{\varepsilon}_i^\nu \left(\hat{C}_{ij}^\nu + \hat{T}_{ij}^\nu \right) \delta \hat{\varepsilon}_j dV = \delta \hat{\pi}_{\text{ext}}^{\nu+1} - \int_{\hat{\Omega}^\nu} \delta \hat{\varepsilon}_i^\nu \hat{\sigma}_j^\nu dV, \quad (93)$$

where \hat{C}_{ij}^ν is the consistent tangent modulus tensor corresponding to pure deformation (see Section 3.2.3) but expanded to a 9 by 9 matrix; \hat{T}_{ij}^ν is the geometric stiffness matrix which is given as follows (Liu (1992)):

$$\mathbf{T} = \begin{bmatrix} \sigma_1 & 0 & 0 & \frac{\sigma_4}{2} & 0 & \frac{\sigma_6}{2} & \frac{\sigma_4}{2} & 0 & -\frac{\sigma_6}{2} \\ & \sigma_2 & 0 & \frac{\sigma_4}{2} & \frac{\sigma_5}{2} & 0 & -\frac{\sigma_4}{2} & \frac{\sigma_5}{2} & 0 \\ & & \sigma_3 & 0 & \frac{\sigma_5}{2} & \frac{\sigma_6}{2} & 0 & -\frac{\sigma_5}{2} & \frac{\sigma_6}{2} \\ & & & \frac{\sigma_1+\sigma_2}{4} & \frac{\sigma_6}{4} & \frac{\sigma_5}{4} & \frac{\sigma_2-\sigma_1}{4} & \frac{\sigma_6}{4} & -\frac{\sigma_5}{4} \\ & & & & \frac{\sigma_2+\sigma_3}{4} & \frac{\sigma_4}{4} & -\frac{\sigma_6}{4} & \frac{\sigma_3-\sigma_2}{4} & \frac{\sigma_4}{4} \\ & & \text{symm.} & & & \frac{\sigma_1+\sigma_3}{4} & \frac{\sigma_5}{4} & -\frac{\sigma_4}{4} & \frac{\sigma_1-\sigma_3}{4} \\ & & & & & & \frac{\sigma_1+\sigma_2}{4} & -\frac{\sigma_6}{4} & -\frac{\sigma_5}{4} \\ & & & & & & & \frac{\sigma_2+\sigma_3}{4} & -\frac{\sigma_4}{4} \\ & & & & & & & & \frac{\sigma_3+\sigma_1}{4} \end{bmatrix}. \quad (94)$$

By interpolation

$$\Delta \mathbf{u} = \mathbf{N} \Delta \mathbf{d}, \quad \delta \mathbf{u} = \mathbf{N} \delta \mathbf{d}; \quad (95)$$

$$\Delta \boldsymbol{\varepsilon} = \bar{\mathbf{B}} \Delta \mathbf{d}, \quad \delta \boldsymbol{\varepsilon} = \bar{\mathbf{B}} \delta \mathbf{d}, \quad (96)$$

where \mathbf{N} and $\bar{\mathbf{B}}$ are, respectively, the shape functions and strain operators defined in Section 2. This leads to a set of equations

$$\hat{\mathbf{K}}^\nu \Delta \hat{\mathbf{d}} = \hat{\mathbf{r}}^{\nu+1} = \hat{\mathbf{f}}_{\text{ext}}^{\nu+1} - \hat{\mathbf{f}}_{\text{int}}^\nu, \quad (97)$$

where the tangent stiffness matrix, $\hat{\mathbf{K}}^\nu$, and the internal nodal force vector, $\hat{\mathbf{f}}_{\text{int}}^\nu$, are

$$\hat{\mathbf{K}}^\nu = \int_{\hat{\Omega}^\nu} \hat{\mathbf{B}}^t (\hat{\mathbf{C}}^\nu + \hat{\mathbf{T}}^\nu) \hat{\mathbf{B}} dV, \quad (98)$$

$$\hat{\mathbf{f}}_{\text{int}}^\nu = \int_{\hat{\Omega}^\nu} \hat{\mathbf{B}}^t \hat{\boldsymbol{\sigma}}^\nu dV. \quad (99)$$

The tangent stiffness and nodal force are transformed into the global coordinate system tensorially as

$$\mathbf{K}^\nu = \mathbf{R}^{\nu t} \hat{\mathbf{K}}^\nu \mathbf{R}^\nu, \quad (100)$$

$$\mathbf{r}^{\nu+1} = \mathbf{R}^{\nu t} \hat{\mathbf{f}}_{\text{int}}^\nu, \quad (101)$$

where \mathbf{R}^ν is the transformation matrix of the corotational system defined by \mathbf{x}_{n+1}^ν . Finally we get a set of linear algebraic equations

$$\mathbf{K}^\nu \Delta \mathbf{d}^{\nu+1} = \mathbf{r}^{\nu+1}. \quad (102)$$

NUMERICAL EXAMPLES

To investigate the performance of the element introduced in this paper, a variety of problems including linear elastic and nonlinear elastic-plastic/large deformation problems are studied. Since the element is developed to avoid locking, the applicability to problems of thin structures is studied by solving the standard test problems including pinched cylinder and Scordelis-Lo roof, which are proposed by MacNeal, 1985 and Belytschko, 1984b. Also a sheet metal forming problem is solved to test and demonstrate the effectiveness and efficiency of this element.

Timoshenko Cantilever Beam

The first problem is a linear, elastic cantilever beam with a load at its end as shown in Fig. 4, where M and P at the left end of the cantilever are reactions at the support. The analytical solution from Timoshenko, 1970 is

$$u_x(x, y) = \frac{-Py}{6\bar{E}I} [(6L - 3x)x + (2 + \bar{\nu})(y^2 - \frac{1}{4}D^2)], \quad (103)$$

$$u_y(x, y) = \frac{P}{6\bar{E}I} [3\bar{\nu}y^2(L - x) + \frac{1}{4}(4 + 5\bar{\nu})D^2x + (3L - x)x^2], \quad (104)$$

where

$$I = \frac{1}{12}D^3,$$

$$\bar{E} = \begin{cases} E, & \text{for plane stress;} \\ E/(1 - \nu^2), & \text{for plane strain.} \end{cases} \quad \bar{\nu} = \begin{cases} \nu, & \text{for plane stress;} \\ \nu/(1 - \nu), & \text{for plane strain.} \end{cases}$$

The displacements at the support end, $x = 0$, $-\frac{1}{2}D \leq y \leq \frac{1}{2}D$ are nonzero except at the top, bottom and midline (as shown in Fig. 5). Reaction forces are applied at the support based on the stresses corresponding to the displacement field at $x = 0$, which are

$$\sigma_{xx} = -\frac{Py}{I}(L - x), \quad \sigma_{yy} = 0, \quad \sigma_{xy} = \frac{P}{2I}(\frac{1}{4}D^2 - y^2). \quad (105)$$

The distribution of the applied load to the nodes at $x = L$ is also obtained from the closed-form stress fields.

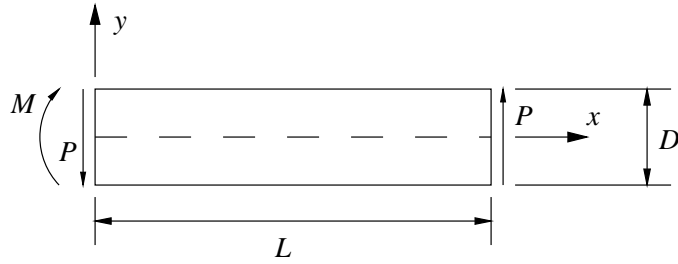
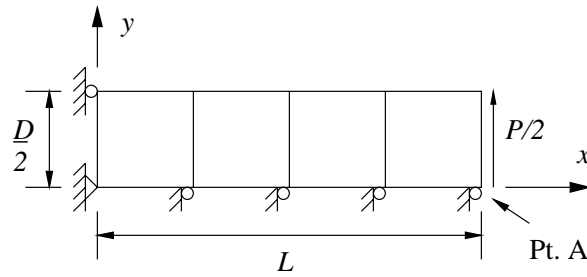
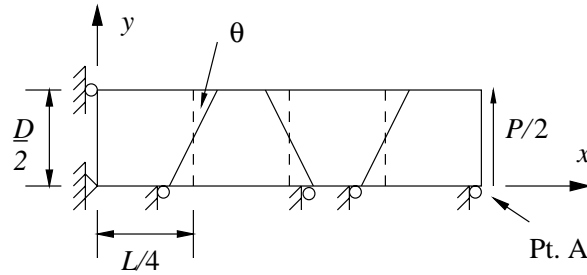


Figure 4: Timoshenko cantilever beam.



(a) Regular mesh



(b) Skewed mesh

Figure 5: Top half of antisymmetric beam mesh

The parameters for the cantilever beam are: $L = 1.0$, $D = 0.02$, $P = 2.0$, $E = 1 \times 10^7$; and two values of Poisson's ratio: (1) $\nu = 0.25$, (2) $\nu = 0.4999$.

Since the problem is antisymmetric, only the top half of the beam is modeled. Plane strain conditions are assumed in the z -direction and only one layer of elements is used in this direction. Both regular mesh and skewed mesh are tested for this problem.

Normalized vertical displacements at point A for each case are given in Tables 1. Tables 1a and 1b show the normalized displacement at point A for the regular mesh. There is no shear or volumetric locking for this element. For the skewed mesh, with the skewed angle increased, we need more elements to get more accurate solution (Table 1c).

Pinched Cylinder

Figure 6 shows a pinched cylinder subjected to a pair of concentrated loads. Two cases are studied in this example. In the first case, both ends of the cylinder are assumed to be free. In the second case, both ends of the cylinder are covered with rigid diaphragms so that only the displacement in the axial direction is allowed at the ends. The parameters for the first case

Table 1: Normalized displacement at point A of cantilever beam

(a) $\nu = 0.25$, regular mesh

analytical solution $w_A = 9.3777 \times 10^{-2}$

| Mesh | $4 \times 1 \times 1$ | $8 \times 1 \times 1$ | $8 \times 2 \times 1$ |
|-------|-----------------------|-----------------------|-----------------------|
| HEXDS | 1.132 | 1.142 | 1.029 |

(b) $\nu = 0.4999$, regular mesh

analytical solution $w_A = 7.5044 \times 10^{-2}$

| Mesh | $4 \times 1 \times 1$ | $8 \times 1 \times 1$ | $8 \times 2 \times 1$ |
|-------|-----------------------|-----------------------|-----------------------|
| HEXDS | 1.182 | 1.197 | 1.039 |

(c) $\nu = 0.25$, skewed mesh

| θ | 1° | 5° | 10° |
|------------------------|-----------|-----------|------------|
| $4 \times 1 \times 1$ | 1.078 | 0.580 | 0.317 |
| $8 \times 1 \times 1$ | 1.136 | 0.996 | 0.737 |
| $16 \times 1 \times 1$ | 1.142 | 1.090 | 0.955 |

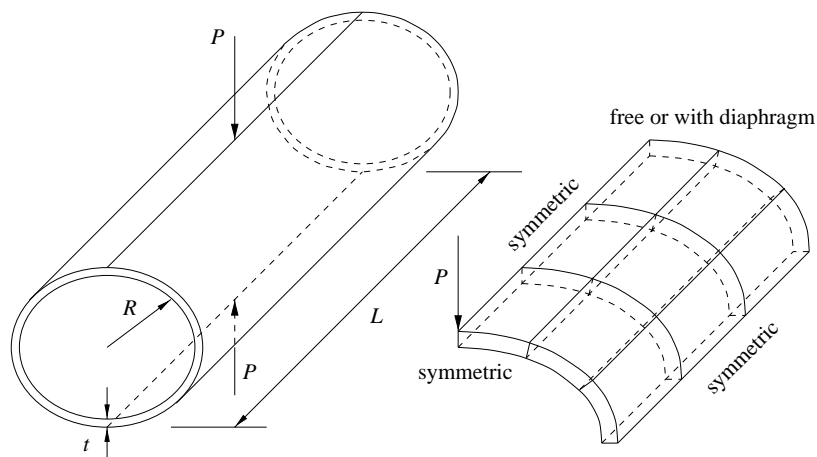


Figure 6: Pinched cylinder and the element model

(without diaphragms) are

$$E = 1.05 \times 10^6, \nu = 0.3125, L = 10.35, R = 1.0, t = 0.094, P = 100.0;$$

while for the second case (with diaphragms), the parameters are set to be

$$E = 3 \times 10^6, \nu = 0.3, L = 600.0, R = 300.0, t = 3.0, P = 1.0.$$

Due to symmetry only one octant of the cylinder is modeled. The computed displacements at the loading point are compared to the analytic solutions in Table 2. HEXDS element works well in both cases, indicating that this element can avoid not only shear locking but also membrane locking; this is not unexpected since membrane locking occurs primarily in curved elements (Stolarski, 1983).

Scordelis-Lo Roof

Scordelis-Lo roof subjected to its own weight is shown in Figure 7. Both ends of the roof

Table 2: Normalized displacement at loading point of pinched cylinder

(a) First case without diaphragms

Analytical solution $w_{\max} = 0.1137$

| Mesh | $10 \times 10 \times 2$ | $16 \times 16 \times 4$ | $20 \times 20 \times 4$ |
|-------|-------------------------|-------------------------|-------------------------|
| HEXDS | 1.106 | 1.054 | 1.067 |

(a) Second case with diaphragms

Analytical solution $w_{\max} = 1.8248 \times 10^{-5}$

| Mesh | $10 \times 10 \times 2$ | $16 \times 16 \times 4$ | $20 \times 20 \times 4$ |
|-------|-------------------------|-------------------------|-------------------------|
| HEXDS | 0.801 | 0.945 | 0.978 |

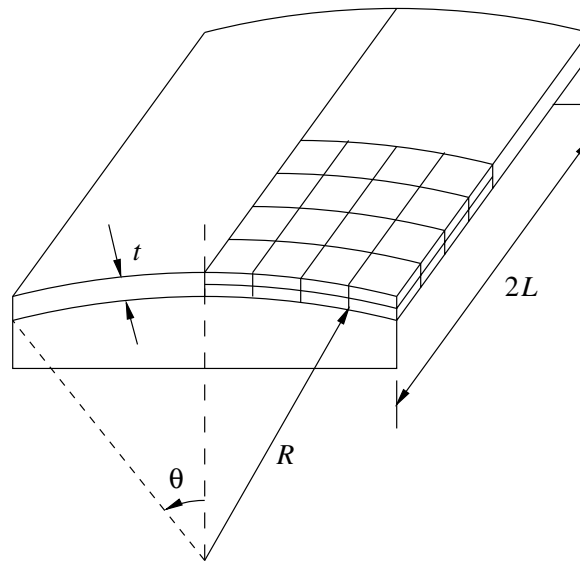


Figure 7: Scordelis-Lo roof under self weight

are assumed to be covered with rigid diaphragms. The parameters are selected to be: $E = 4.32 \times 10^8$, $\nu = 0.0$, $L = 50.0$, $R = 25.0$, $t = 0.25$, $\theta = 40^\circ$, and the gravity is 360.0 per volume.

Due to symmetry only one quarter of the roof is modeled. The computed displacement at the midpoint of the edge is compared to the analytic solution in Table 3. In this example the HEXDS element can get good result with 100×2 elements.

Table 3: Normalized displacement at mid-edge of Scordelis-Lo roof

Analytical solution $w_{\max} = 0.3024$

| Mesh | $8 \times 8 \times 1$ | $16 \times 16 \times 1$ | $32 \times 32 \times 1$ | $10 \times 10 \times 2$ |
|-------|-----------------------|-------------------------|-------------------------|-------------------------|
| HEXDS | 1.157 | 1.137 | 1.132 | 1.045 |

Circular Sheet Stretched with a Tight Die

A circular sheet is stretched under a hemisphere punch and a tight die with a small corner radius (Fig. 8). The material is elastoplastic with nonlinear hardening rule. The elastic material con-

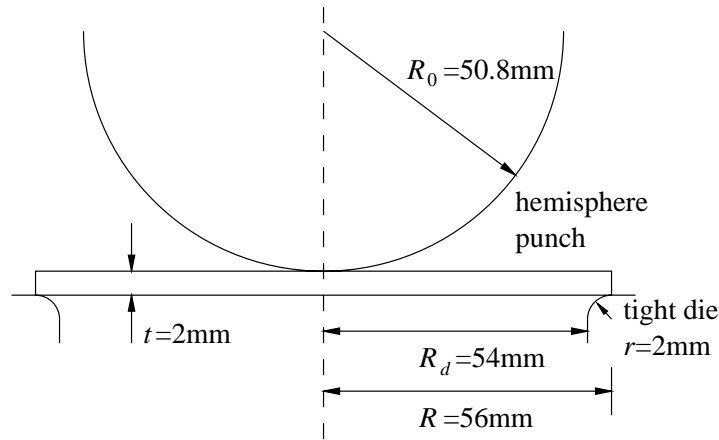


Figure 8: Circular sheet stretched with a tight die

stants are: $E = 206 \text{ GPa}$ and $\nu = 0.3$. In the plastic range, the uniaxial stress-strain curve is given by

$$\sigma = K \varepsilon^n,$$

where $K = 509.8 \text{ MPa}$, $n = 0.21$, σ is Cauchy stress and ε is natural strain (logarithmic strain). The initial yield stress is obtained to be $\sigma_0 = 103.405 \text{ MPa}$ and the tangent modulus at the initial yield point is $E_t = 0.4326 \times 10^5 \text{ MPa}$.

Because of the small corner radius of the die, the same difficulties as in the problem of sheet stretch under the rigid cylinders lead the shell elements to failure in this problem. Three dimensional solid elements are needed and fine meshes should be put in the areas near the center and the edge of the sheet.

One quarter of the sheet is modeled with 1400×2 HEXDS elements due to the double symmetries. The mesh is shown in Fig. 9. Two layers of elements are used in the thickness. Around the center and near the circular edge of the sheet, fine mesh is used. The nodes on the edge are fixed in x - and y -directions and the bottom nodes on the edge are prescribed in three directions. No friction is considered in this simulation. For comparison, the axisymmetric four-node element with reduced integration (CAX4R) is also used and the mesh for this element is the same as shown in the top of Figure 9.

The results presented here are after the punch has traveled down 50 mm. The profile of the circular sheet is shown in Figure 10 where we can see that the sheet under the punch experiences most of the stretching and the thickness of the sheet above the die changes a lot. The deformation between the punch and the die is small. However, the sheet thickness obtained by the CAX4R element is less than that by the HEXDS element and there is slight difference above the die. These observations can be verified by the strain distributions in the sheet along the radial direction (Figures 12). The direction of the radial strain is the tangent of the mid-surface of the element in the rz plane and the thickness strain is in the direction perpendicular to the mid-surface of the element. The unit vector of the circumferential strain is defined as the cross-product of the directional cosine vectors of the radial strain and the thickness strain. We can see that the CAX4R element yields larger strain components in the area under the punch than the HEXDS element. The main difference of the strain distributions in the region above the die is that the CAX4R element gives zero circumferential strain in this area but the HEXDS element

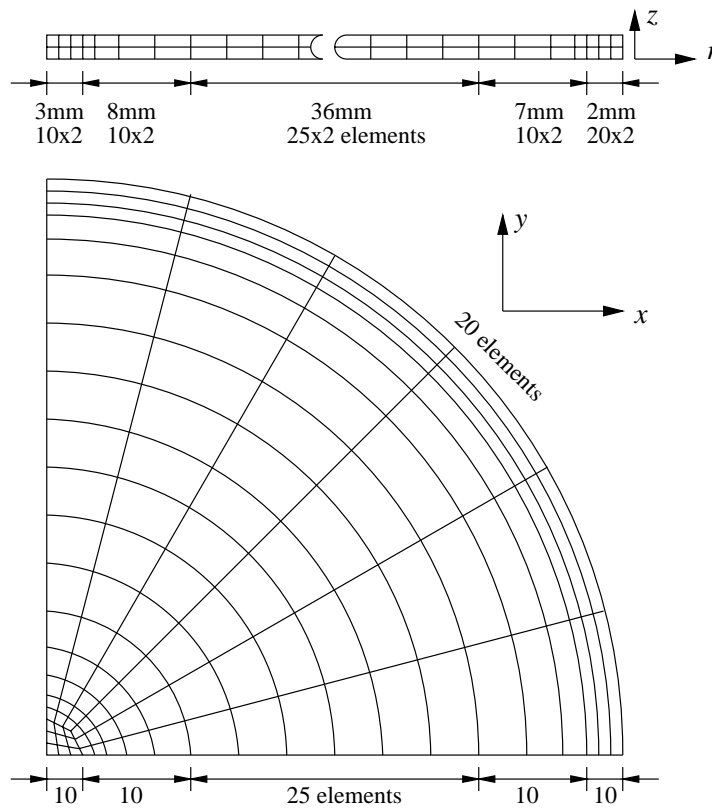


Figure 9: Mesh for circular sheet stretching

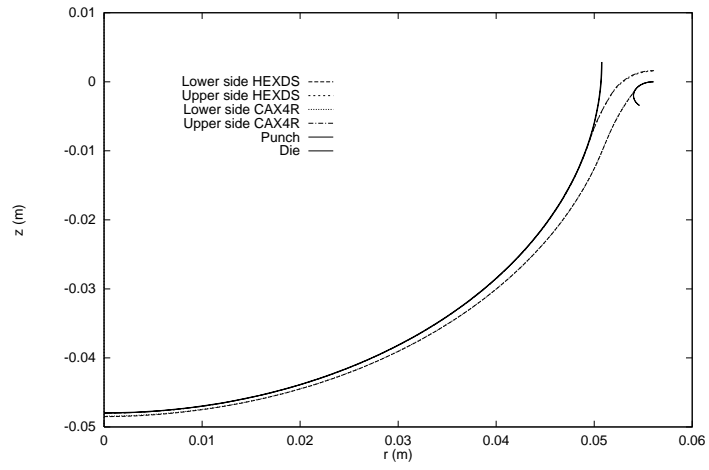


Figure 10: Deformed shape of a circular sheet with punch travel 50 mm

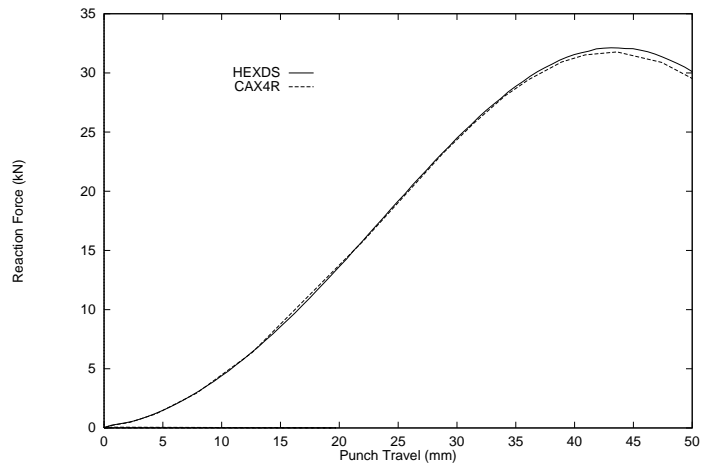
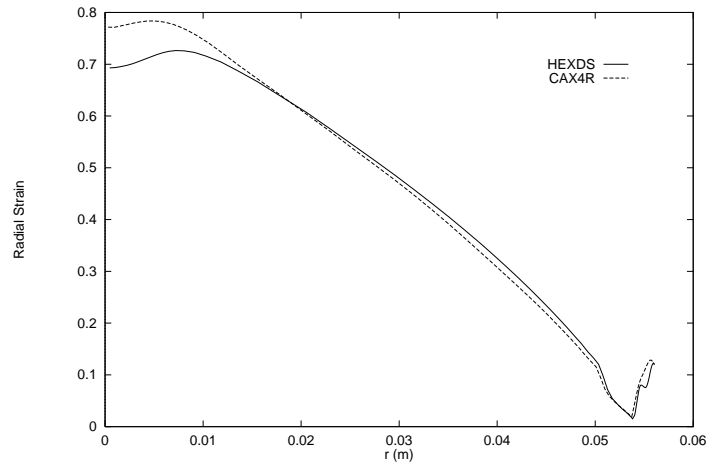
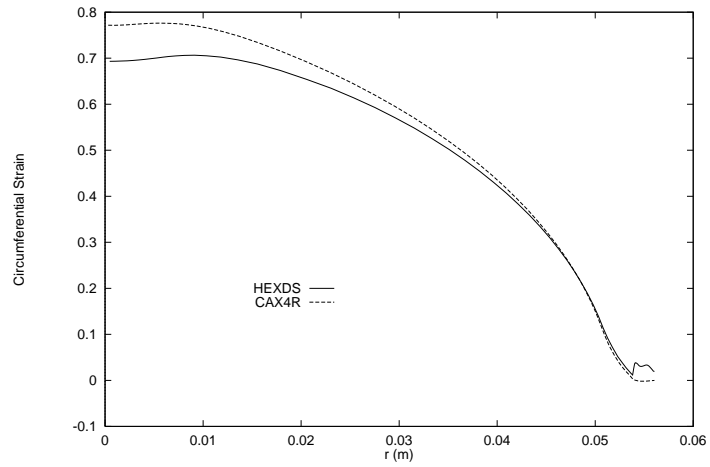


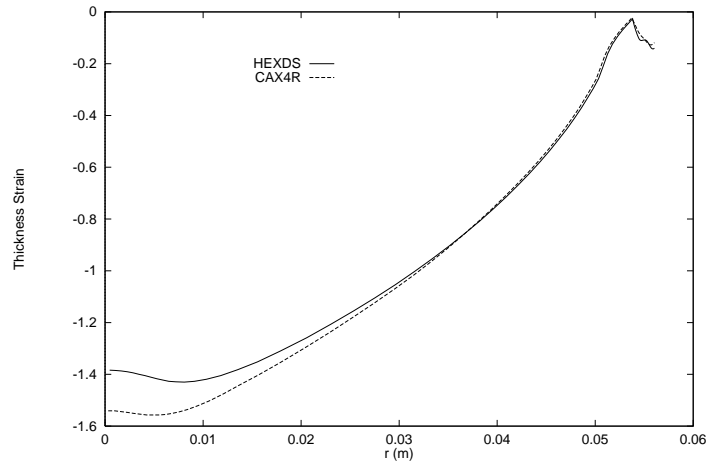
Figure 11: Reaction force vs punch travel for the circular sheet



(a) Radial strain distribution



(b) Circumferential strain distribution



(c) Thickness strain distribution

Figure 12: Strain distributions in circular sheet with punch travel 50 mm

yields non-zero strain. The value of the reaction force shown in the Figure 11 is only one quarter of the total punch reaction force since only one quarter of the sheet is modeled. From this figure we can see that the sheet begins softening after the punch travels down about 45 mm, indicating that the sheet may have necking though this cannot be seen clearly from Figure 10.

CONCLUSIONS

A new eight-node hexahedral element is implemented for the large deformation elastic-plastic analysis. Formulated in the corotational coordinate system, this element is shown to be effective and efficient and can achieve fast convergence in solving a wide variety of nonlinear problems.

By using a corotational system which rotates with the element, the locking phenomena can be suppressed by omitting certain terms in the generalized strain operators. In addition, the integration of the constitutive equation in the corotational system takes the same simple form as small deformation theory since the stress and strain tensors defined in this corotational system are objective.

Radial return algorithm is used to integrate the rate-independent elastoplastic constitutive equation. The tangent stiffness matrix consistently derived from this integration scheme is crucial to preserve the second order convergence rate of the Newton's iteration method for the nonlinear static analyses.

Test problems studied in this paper demonstrate that the element is suitable to continuum and structural numerical simulations. In metal sheet forming analysis, this element has advantages over shell elements for certain problems where through the thickness deformation and strains are significant.

REFERENCES

- Belytschko, T. and Hsieh, B.J. (1973), "Nonlinear Transient Finite Element Analysis with Convected Coordinates," *Int. J. Num. Meths. Engrg.*, Vol.7, pp. 255–271.
- Belytschko, T., Lin, J.I. and Tsay, C.S. (1984a), "Explicit Algorithms for the Nonlinear Dynamics of Shells," *Comput. Meths. Appl. Mech. Engrg.*, Vol.42, pp. 225–251.
- Belytschko, T., Ong, J. S.-J., Liu, W.K. and Kennedy, J.M. (1984b), "Hourglass Control in Linear and Nonlinear Problems", *Comput. Meths. Appl. Mech. Engrg.*, Vol.43, pp. 251–276.
- Flanagan, D.P. and Belytschko, T. (1981), "A Uniform Strain Hexahedron and Quadrilateral with Orthogonal Hourglass Control," *Int. J. Num. Meths. Engrg.*, Vol.17, pp. 679–706.
- Hallquist, J.O. (1998), *LS-DYNA Theoretical Manual*, May, 1998.
- Hughes, T.J.R. and Liu, W.K. (1981a), "Nonlinear Finite Element Analysis of Shells: Part I. Three-dimensional Shells," *Comput. Meths. Appl. Mech. Engrg.*, Vol.26, pp. 331–362.
- Hughes, T.J.R. and Liu, W.K. (1981b), "Nonlinear Finite Element Analysis of Shells: Part II. Two-dimensional Shells," *Comput. Meths. Appl. Mech. Engrg.*, Vol.27, pp. 167–181.
- Liu, W.K. and Belytschko, T. (1984), "Efficient Linear and Nonlinear Heat Conduction with a Quadrilateral Element," *Int. J. Num. Meths. Engrg.*, Vol.20, pp. 931–948.

Liu, W.K., Belytschko, T., Ong, J.S.J. and Law, E. (1985), "Use of Stabilization Matrices in Nonlinear Finite Element Analysis," *Engineering Computations*, Vol.2, pp.47–55.

Liu, W.K. (1992), *Lecture Notes on Nonlinear Finite Element Methods*, Northwestern University, 1983, revised in 1992.

Liu, W.K., Hu, Y.K., and Belytschko, T. (1994), "Multiple Quadrature Underintegrated Finite Elements," *Int. J. Num. Meths. Engrg.*, Vol. 37, pp. 3263–3289.

Liu, W.K., Guo, Y., Tang, S. and Belytschko T. (1998), "A Multiple-quadrature Eight-node Hexahedral Finite Element for Large Deformation Elastoplastic Analysis," *Comput. Meths. Appl. Mech. Engrg.*, Vol.154, pp. 69–132.

MacNeal R.H. and Harder R.L. (1985), "A Proposed Standard Set of Problems to Test Finite Element Accuracy," *Finite Elements Anal. Des.*, Vol. 11, pp. 3–20.

Stolarski, H. and Belytschko, T. (1983), "Shear and Membrane locking in curved elements," *Comput. Meths. Appl. Mech. Engrg.*, Vol.41, pp.279–296.